CrossMark

Thermodynamic complexity of sulfated zirconia catalysts

Naiwang Liu [a,b], Xiaofeng Guo [c], Alexandra Navrotsky [b,*], Li Shi [a,*], Di Wu [d,*]

[a] State Key Laboratory of Chemical Engineering, East China University of Science and Technology, Shanghai 200237, China
[b] Peter A. Rock Thermochemistry Laboratory and NEAT ORU, University of California, Davis, One Shields Avenue, Davis, CA 95616, United States
[c] Earth System Observations, Earth and Environmental Sciences Division, Los Alamos National Laboratory, Los Alamos, NM 87545, United States
[d] The Gene and Linda Voiland School of Chemical Engineering and Bioengineering, Washington State University, Pullman, WA 99163, United States

A B S T R A C T

A series of sulfated zirconia (SZ) catalysts were synthesized by immersion of amorphous zirconium hydroxide in sulfuric acid of various concentrations (1–5 N). These samples were fully characterized by X-ray diffraction (XRD), thermogravimetric analysis and mass spectrometry (TGA-MS), and aqueous sulfuric acid immersion and high temperature oxide melt solution calorimetry. We investigated the enthalpies of the complex interactions between sulfur species and the zirconia surface (ΔH_{SZ}) for the sulfated zirconia precursor (SZP), ranging from -109.46 ± 7.33 (1 N) to -42.50 ± 0.89 (4 N) kJ/mol S. ΔH_{SZ} appears to be a roughly exponential function of sulfuric acid concentration. On the other hand, the enthalpy of SZ formation (ΔH_f), becomes more exothermic linearly as sulfur surface coverage increases, from -147.90 ± 4.16 (2.14 nm^{-2}) to -317.03 ± 4.20 (2.29 nm^{-2}) kJ/mol S, indicating formation of energetically more stable polysulfate species.

© 2016 Elsevier Inc. All rights reserved.

1. Introduction

Heterogeneous catalysis plays a critical role in modern chemical industry. Unless the catalytic active components are stabilized through subtle, thermodynamically favorable interactions on a substrate they are generally not robust for industrial applications [1]. Well-known examples include supported metal nanoclusters [2] and dispersed super-acidic moieties [3]. Thus, knowing the strength of interactions and bonding between molecular-level active catalytic species and support materials is of great importance for understanding and optimizing parameters for successful catalyst synthesis and operation.

Because of its very strong surface acidity, sulfated zirconia (SZ) has been applied extensively in the chemical industry as an acid catalyst [4]. Applications include isomerization [5], hydrocracking [6], alkylation [7,8] and oligomerization of hydrocarbons [9]. Numerous experimental (spectroscopy, diffraction and microscopy) [10–14] and computational (density functional theory and molecular dynamics) [15,16] studies have been performed to explore the specific binding, surface assembly and/or structure, and catalytic activity of SZ. However, few studies have investigated the energetics of SZ materials, including sulfur species – zirconia

interactions in aqueous solutions during catalyst precursor (SZP) synthesis (enthalpy of immersion of zirconia in sulfuric acid), the material phase evolution during calcination, and the energetics of formation of the as-made SZ catalyst.

In this context, calorimetry is a powerful tool to probe the interactions and bonding energetics on surfaces or at interfaces. Recently, we have performed a series of systematic thermochemical studies on small molecule – surface interactions using immersion, solution and/or gas adsorption calorimetry [17–21]. In addition, the bonding energetics of CO_2 [22,23], CH_4 [24], water, ethanol [25], N,N-dimethylformamide (DMF) and N,N-diethylformamide (DEF) [26] was also investigated for various metal–organic frameworks (MOFs). Most of these bonding or interaction enthalpies were found to be functions of adsorbate molecule coverage.

Here, we take a similar approach to evaluate interactions in the SZ catalyst. Combining sulfuric acid immersion calorimetry, high temperature oxide melt solution calorimetry, and thermogravimetric analysis and mass spectrometry (TGA-MS), we determined the magnitude of sulfur species – zirconia surface interactions (enthalpy of immersion) under SZP synthesis conditions at room temperature. Additionally, we identified two groups of energetically distinct sulfur species adsorbed on the SZP surface. Further, we quantified the enthalpies of SZ formation (ΔH_f) from constituent oxides. These energetics were determined, interpreted and discussed as functions of sample treatment temperature, sul-

furic acid concentration, and sulfur species coverage. These measurements provide thermodynamic insights for sulfation of zirconia surfaces in both catalytic material synthesis and applications.

2. Materials and methods

2.1. Synthesis of sulfated zirconia (SZ)

Zirconium hydroxide (Z) was synthesized via a sol-gel method. Ammonium hydroxide solution ($\sim$25% v/v) was dripped into zirconium oxychloride ($ZrOCl_2 \cdot 8H_2O$) aqueous solution kept at 60 °C under vigorous stirring until the pH reached 8.0. This solution was aged at room temperature for 12 h followed by filtration. The precipitation, zirconium hydroxide, was collected and washed 5 times to maximize chloride ion removal. The dried zirconium hydroxide powder was then subjected to sulfation immersion/impregnation for 1 h, in which sulfuric acid solutions of different concentration from 1 to 5 N were used. After another round of filtration and drying, we obtained the sulfated zirconia precursor (SZP). The final product, sulfated zirconia (SZ) was achieved through calcination of SZP at 650 °C in air for 2 h. For clarity, the final treatment temperature is marked after each sample name in the tables. Hence, the zirconium hydroxide, sulfated zirconia precursor and sulfated zirconia were denoted with temperature labeled as Z-25, SZP-25 and SZ-650.

2.2. Characterization

Powder X-ray diffraction (XRD) patterns were collected using a Bruker-AXS-D8 Advance diffractometer (Bruker, AXS, Inc., Madison, WI) operated at 40 kV and 40 mA (Cu Kα, λ = 0.15406 nm). Data were acquired in the 2θ range of 20–70° (step size 0.02° and 1 s per step). The sample phase distribution and crystallite size were quantified by Rietveld refinement using JADE 6.1 software.

The Brunauer-Emmett-Teller (BET) surface areas were measured using a Gemini 2360 instrument (Micromeritics, Norcross, GA). Prior to BET analysis, samples were degassed at 200 °C under vacuum for 12 h. All the measurements were triplicated to ensure reproducibility.

2.3. Thermogravimetric analysis and mass spectrometry (TGA-MS)

Thermogravimetric analysis (TGA) was carried out using a Netzsch STA 449 instrument (Netzsch, Selb, Germany). About 20 mg sample was pressed into a pellet and heated from 30 to 1000 °C (10 °C/min) under argon flow (40 mL/min). The evolved gas was introduced into a mass spectrometer (Cirrus-2, MKS Instruments UK Ltd., Crewe, UK) through a capillary tube heated at 100 °C. Each TGA-MS analysis was corrected by recording a baseline with empty platinum crucible. The mass spectrometer was calibrated using calcium oxalate monohydrate ($CaC_2O_4 \cdot H_2O$), which has known water content.

2.4. Immersion calorimetry

The immersion enthalpies of zirconia in sulfuric acid solutions (1–5 N) were measured using a Setaram C80 microcalorimeter (Setaram Instrumentation, Caluire, France) equipped with a custom-made dropping tube. Each sample was hand-pressed into a pellet (about 10 mg), weighed on a microbalance, and dropped from room temperature into the solution at 25 °C. The drop resulted in a heat effect (calorimetric peak) associated with the reaction between the solid sample and the solution. Immersion calorimetry on each sample was repeated at least eight times to ensure reproducibility, which is shown as error bars (2 standard

deviations of the mean) in the figures. Prior to immersion calorimetry, samples were outgassed at 200 °C overnight to maximize removal of adsorbed species.

2.5. High temperature oxide melt solution calorimetry

The drop solution enthalpies of all samples in molten sodium molybdate ($3Na_2O \cdot 4MoO_3$) at 703 °C were measured using a custom-made Tian-Calvet twin microcalorimeter. The detailed methodology was described elsewhere [27]. Sample pellets ($\sim$5 mg) were hand-pressed and dropped from ambient conditions into the solvent in a platinum crucible in the hot calorimeter. The calorimetric assembly was flushed using oxygen (50 mL/min) to maintain oxidizing environment and the solvent was bubbled with oxygen (0.5 mL/min) to promote sample dissolution and to propel evolved gases. All samples were degassed at 200 °C overnight before calorimetric measurement. The calorimeter was calibrated using the known heat content of high purity alpha alumina (Alfa Aesar, 99.997%). The thermodynamic cycles used to derive the enthalpy of SZ formation (ΔH_f) are listed in Table 1.

2.6. Catalytic activity test

An alkylation reaction in which olefins react with aromatics leading to reduced olefin concentration in aromatic liquids (Scheme 1) [31] was employed to test the catalytic activity of SZ treated in different conditions. Alkylation was carried out in a fixed bed tubular micro-reactor equipped with a constant flow pump to enable precise flow rate and temperature control. Catalyst (SZ, 2 mL) was loaded into the micro-reactor, the spare space of which was filled with quartz sand (space filler). The tests were performed at 1.0 MPa with a liquid hourly space velocity (LHSV) of 30 h^{-1} [32]. Bromine Index is an indicator of olefin content in aromatics. According to ASTM standard D 2710-92, it is defined as the amount of bromine (mg) consumed by 100 g of hydrocarbon. The inlet and effluent liquids of the fixed bed tubular micro-reactor were monitored by a Bromine Index Analyzer (OSC 971KK 101, Ogawa Seiki Co., Ltd., Tokyo, Japan). The olefin conversion rate, X, was calculated as $X = (N_i - N_o)/N_i \times 100\%$, in which N_i and N_o correspond to the bromine index of the inlet and effluent liquids, respectively. The specific olefin and aromatic compounds involving in the alkylation reactions and their contents are listed in Table 2 [32].

Table 1
Thermodynamic cycles for enthalpies of SZ formation, ΔH_f.

Reaction formula[a]	Reaction enthalpy
$ZrO_2 \cdot xSO_3 \cdot yH_2O$ (tetragonal/ads/ads, 25 °C) → ZrO_2 (sol, 703 °C) + yH_2O (g, 703 °C) + xSO_3 (sol, 703 °C)[b]	ΔH_{ds}
ZrO_2 (tetragonal, 25 °C) → ZrO_2 (sol, 703 °C)	ΔH_1[c]
H_2O (ads, 25 °C) → H_2O (g, 25 °C)	ΔH_2[d]
H_2O (g, 25 °C) → H_2O (g, 703 °C)	ΔH_3[e]
SO_3 (g, 25 °C) → SO_3 (sol, 703 °C)	ΔH_4[f]
SO_3 (ads, 25 °C) → SO_3 (g, 25 °C)	ΔH_f
$\Delta H_f = \Delta H_{ds} - \Delta H_1 - \Delta H_2 - \Delta H_3 - \Delta H_4$	

[a] "g", "ads" and "sol" denote "gas", "adsorption" and "in sodium molybdate solution", respectively.
[b] Ref. Majzlan et al. [28] and Drouet and Navrotsky [29].
[c] ΔH_{ds} and ΔH_1 (ΔH_1 = 27.06 ± 0.71 kJ/mol ZrO_2 [30]) are drop solution enthalpies of sulfated zirconia (SZ) and nanophase tetragonal zirconia obtained using high temperature oxide melt solution calorimetry, respectively.
[d] ΔH_2 is enthalpy of H_2O adsorption on sulfated zirconia surface.
[e] ΔH_3 = 25.65 kJ/mol H_2O [30].
[f] ΔH_4 is drop solution enthalpy for SO_3, and it cannot be determined directly experimentally but has been calculated from the formation enthalpies of SO_2 and O_2. According to previous work, ΔH_4 = −217.02 ± 4.17 kJ/mol [28].
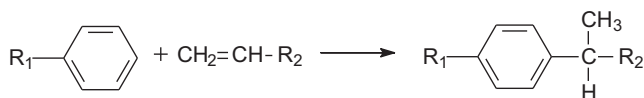
Scheme 1. Alkylation between aromatics and olefins.

Table 2
The specific olefin and aromatic compounds (BI = 1035) involving in the alkylation reactions and their contents.

Compound	Content (wt%)
Nonaromatics	2.08
Benzene	0.06
Toluene	0.05
Ethylbenzene	6.85
p-Xylene	8.92
m-Xylene	18.98
o-Xylene	12.25
C_9	37.12
C_{10} and $C_{10}+$	13.69

Fig. 2. Mass spectrometry (MS) curves of H_2O, SO_2 and O_2 for SZP-25 (4 N) sample.

3. Results

3.1. Characterization

The TGA and DTG traces and corresponding MS curves of SZP-25 (4 N) are presented in Figs. 1 and 2. MS signals were observed for M/Z = 18, 32 and 64, which correspond to H_2O, O_2 and SO_2, respectively. Thermal analysis of SZP-25 in argon results in a series of reactions, which can be categorized into two groups. H_2O is desorbed from the SZP surface first. There appears to be two types of energetically distinct H_2O species. Physisorbed H_2O is released at about 120 °C, while liberation of chemisorbed H_2O takes place between 300 and 500 °C. This is followed by decomposition of sulfur species from 600 to 850 °C, leading to evolution of SO_2 and O_2 (SO_2: $O_2 \sim 2:1$). The position, shape and area of MS peaks for H_2O, O_2 and SO_2 correspond very well with the TGA and DTG curves (Figs. 1 and 2).

The SO_2 MS signal of SZP-25 (4 N) was further interpreted in detail to reveal the energetic insights into sulfur species – zirconia surface interactions in SZ catalyst synthesis (see Fig. 3). SZP-25 (4 N) presents two overlapped SO_2 MS peaks upon heating to 1000 °C. Applying Gaussian multi-peak fitting, we were able to split this signal into two peaks (Fig. 3A). The first peak is sharp, centered at approximately 650 °C, while the second peak is broad,
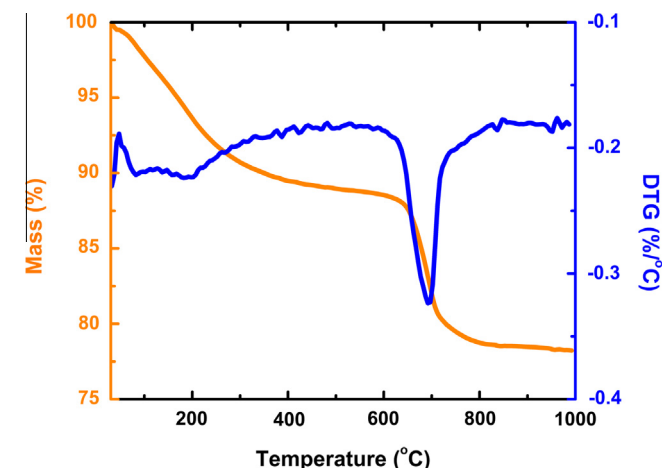

Fig. 3. Separation of SO_2 mass spectrometry (MS) signals for SZP-25 (4 N) sample.

spanning 600 to 850 °C. We also attempted to separate these two peaks by "quenching" the SZ sample at about 650 °C, followed by another round of TGA-MS examination using the same experimental conditions (see Fig. 3B and C). These results clearly suggest two types of energetically distinct sulfuric components on ZrO_2.

The XRD patterns of Z-25, SZP-25, Z-650, SZ-650, SZ-720 and SZ-1000 are plotted in Fig. 4. These SZP and SZ samples had been prepared using 4 N sulfuric acid. At 25 °C, both Z-25 and SZP-25 are amorphous. Upon calcination at 650 °C in air, Z-650 crystallized to monoclinic zirconia, while SZ-650 became a mixture of monoclinic and tetragonal phases. SZ-720 became completely tetragonal as temperature increased to 720 °C. Ultimately, all samples became monoclinic after calcination at 1000 °C. Sample compositions are listed in Tables 3 and 4. BET surface areas for all samples are listed in Table 4. The sample surface area tends to increase as sulfuric acid concentration increases, ranging from 56.19 ± 0.18 (1 N) to 84.85 ± 0.38 (5 N) m^2/g.

The MS traces, collected from room temperature to 1000 °C, of SZP-25 and SZ-650 prepared with sulfuric acid of different concentration ($C_s = 1–5$ N) are presented in Fig. 5. The MS profiles of SZP-25 and SZ-650 exhibit distinctly different behavior as a function of C_s. Generally, the loading of sulfur species on the SZP-25 surface ($C_{surface}$) is proportional to the sulfuric acid concentration C_s. There

Fig. 1. Thermogravimetric analysis (TGA) and differential thermogravimetric analysis (DTG) profiles for SZP-25 (4 N) sample.
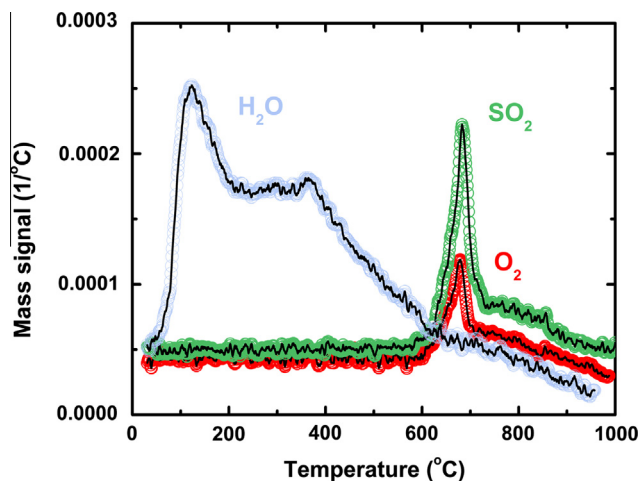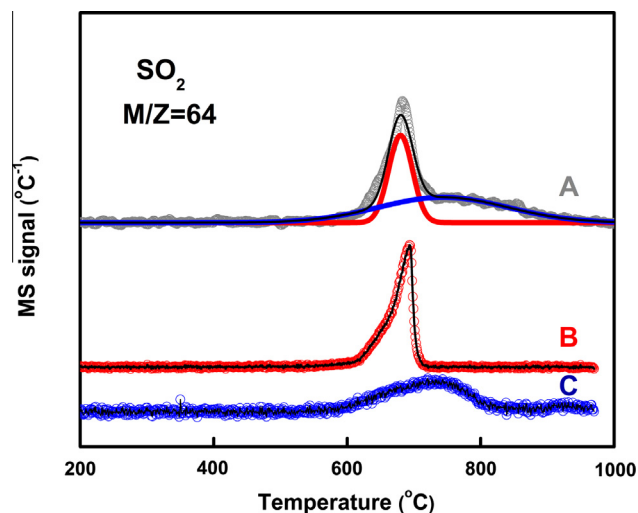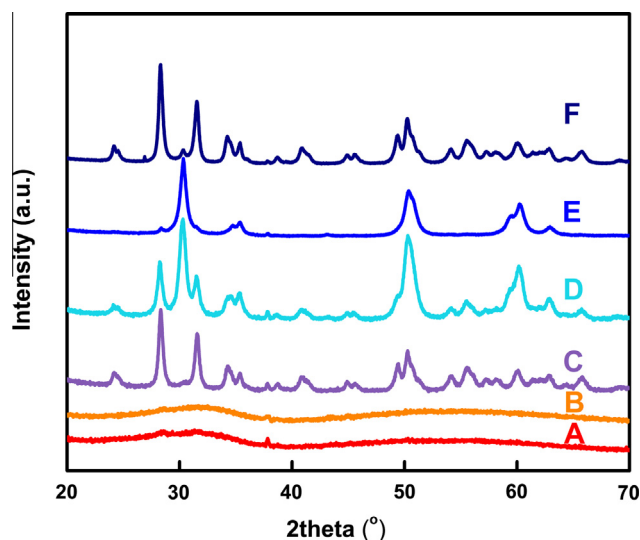
Fig. 4. Powder X-ray diffraction (XRD) patterns of (A) pure zirconia at 25 °C (Z-25), (B) sulfated zirconia precursor (SZP-25) 25 °C, (C) pure zirconia at 650 °C (Z-650), (D) sulfated zirconia at 650 °C (SZ-650), (E) sulfated zirconia at 720 °C (SZ-720), and (F) sulfated zirconia at 1000 °C (SZ-1000).

are two peaks for SZP-25 samples. As C_s increases, the height or intensity of the first peak centered at about 650 °C increases. In sharp contrast, there is only one peak for SZ-650 samples. The MS intensity and peak area for SZ-650 samples do not change for C_s higher than 2 N.

3.2. Immersion calorimetry

The immersion calorimetry data are plotted in Fig. 6. All immersion enthalpies are exothermic, confirming stabilizing surface interactions between zirconia and sulfate species. The enthalpy of immersion of pure zirconia (Z-25) tends to become less exothermic as the concentration of sulfuric acid increases from 1 to 5 N, ranging from −109.46 ± 7.33 (1 N) to −42.50 ± 0.89 (4 N) kJ per mole of sulfur unit (kJ/mol S). This plot levels at about −42 kJ/mol S and further increase of sulfuric acid concentration above 3 N does not lead to less exothermic enthalpy of immersion.

3.3. High temperature oxide melt solution calorimetry

The enthalpy of drop solution (ΔH_{ds}, kJ/mol ZrO_2) tends to be more endothermic, values ranging from 18.34 ± 3.04 to 23.47 ± 1.85 kJ/mol ZrO_2, as C_s increases from 1 to 5 N. Considering both sulfation and hydration factors and using the thermodynamic cycle listed in Table 1, we were able to calculate the enthalpy of SZ formation from constituent oxides (ΔH_f, kJ/mol S). The SZ formation enthalpy becomes more exothermic as the sulfur coverage increases, ranging from −147.90 ± 4.16 to −317.03 ± 4.20 kJ/mol S (Fig. 7). From a thermodynamic standpoint, this is reasonable in that, at lower sulfur coverage, only the zirconia surface sites are

filled, while as coverage increases, states more favorable in energy, or representing stronger interactions among sulfate moieties themselves rather than interactions with the surface, become dominant.

3.4. Catalytic activity test

Figs. 8 and 9 show the olefins conversion as a function of the time on stream (TOS). Without anchored sulfur species, the bare zirconia surface does not have catalytic activity. All SZ samples show decreasing olefin conversion as a function of TOS. For a particular TOS, the olefin conversion increases as the calcination temperature increases from 500 to 650 °C. Beyond 700 °C, the SZ catalysts suffer from significant deactivation due to loss of sulfur species (Fig. 8). The SZ samples treated by sulfuric acid with higher concentration show better olefin conversion at the same TOS (Fig. 9). The catalytic activity enhancement reaches a maximum at C_s = 4 N. Further increase of C_s does not result in better performance.

4. Discussion

4.1. Surface – structure – activity relations: calcination of SZP-25 (4 N)

SZP-25 (4 N) was reported to have optimized performance for conversion of olefins (%) [8]. TGA-MS analysis was carried out on this sample to mimic the calcination process in SZ catalyst synthesis. Our results highlight the interplay and competition between surface chemistry and structural evolution as a function of temperature. The desorption/decomposition of the sample occurs in two major temperature ranges (Figs. 1 and 2). The first step takes place between 100 and 300 °C due to slow yet noticeable desorption of water. In this temperature range, dehydration does not result in phase transition (see Fig. 4). Although it is difficult to differentiate physisorbed and chemisorbed water on the TGA trace, clear signal splitting can be identified from the MS curve of water (Fig. 2).

In sharp contrast, in the second step (600–850 °C) both significant weight loss on TGA curve, and well resolved SO_2 and O_2 MS traces corresponding to detachment of sulfur species are observed. In this range, the XRD patterns of SZ at 650 °C (monoclinic and tetragonal) and 720 °C (tetragonal) strongly suggest that sulfur removal not only leads to sulfur species decomposition on the surface, but also significantly modifies the bulk zirconia structure (Fig. 4). For pure zirconia heated at 650 °C (Z-650), tetragonal phase is not observed. This strongly suggests that the surface bonded sulfur species play a crucial role in zirconia phase selection at high temperature (600–850 °C) through significant modification of the structure and energetic states of the surface. Indeed, various studies report that the tetragonal phase is necessary for SZ catalytic activity [33], especially for isomerization of hydrocarbons, for which sulfated monoclinic zirconia exhibits undetectable activity. Similar behavior, with little catalytic activity for SZ-500 (monoclinic), was observed in the alkylation reactions (olefins removal from aromatics) carried out in the present study (Fig. 8). Moreover, the well-separated sulfur MS peaks of SZP-25 (4 N) indicate that

Table 3
Post immersion calorimetry SZP sample compositions and enthalpies of sulfur species – zirconia interactions (ΔH_{SZ}, with different units). These enthalpies data come directly from immersion calorimetry.

Sample	Composition	ΔH_{SZ} (kJ/mol ZrO_2)	ΔH_{SZ} (J/g ZrO_2)	ΔH_{SZ} (kJ/mol S)
SZP-25 (1 N)	$ZrO_2 \cdot 0.07SO_3 \cdot 0.49H_2O$	−7.94 ± 0.53	−57.54 ± 3.85	−109.46 ± 7.33
SZP-25 (2 N)	$ZrO_2 \cdot 0.09SO_3 \cdot 0.56H_2O$	−7.79 ± 0.60	−55.50 ± 4.29	−87.64 ± 6.78
SZP-25 (3 N)	$ZrO_2 \cdot 0.15SO_3 \cdot 1.03H_2O$	−8.09 ± 0.53	−52.35 ± 3.41	−51.31 ± 3.35
SZP-25 (4 N)	$ZrO_2 \cdot 0.20SO_3 \cdot 1.09H_2O$	−8.55 ± 0.18	−53.78 ± 1.13	−42.50 ± 0.89
SZP-25 (5 N)	$ZrO_2 \cdot 0.20SO_3 \cdot 1.11H_2O$	−8.64 ± 0.28	−54.17 ± 1.78	−42.55 ± 1.40

Table 4

Sample characterization and thermodynamic data for high temperature oxide melt solution calorimetry, including enthalpies of dissolution directly measured by calorimetry, ΔH_{ds} and enthalpies of SZ formation, ΔH_f, calculated using thermodynamic cycle listed in Table 1.

| Sample	Composition	Surface Area (m^2/g)	S coverage (nm^{-2})	ΔH_{ds} (kJ/mol ZrO_2)	ΔH_f (kJ/mol S)
SZ-650 (1 N)	$ZrO_2 \cdot 0.02SO_3 \cdot 0.07H_2O$	56.19 ± 0.18	2.29	18.34 ± 0.56	−317.03 ± 4.20
SZ-650 (2 N)	$ZrO_2 \cdot 0.03SO_3 \cdot 0.07H_2O$	67.18 ± 0.19	2.28	16.79 ± 0.43	−305.30 ± 4.18
SZ-650 (3 N)	$ZrO_2 \cdot 0.03SO_3 \cdot 0.09H_2O$	73.68 ± 0.23	2.20	19.66 ± 0.11	−230.61 ± 4.16
SZ-650 (4 N)	$ZrO_2 \cdot 0.04SO_3 \cdot 0.13H_2O$	83.19 ± 0.47	2.16	22.26 ± 0.84	−187.81 ± 4.24
SZ-650 (5 N)	$ZrO_2 \cdot 0.04SO_3 \cdot 0.13H_2O$	84.85 ± 0.38	2.14	23.47 ± 0.43	−147.90 ± 4.16
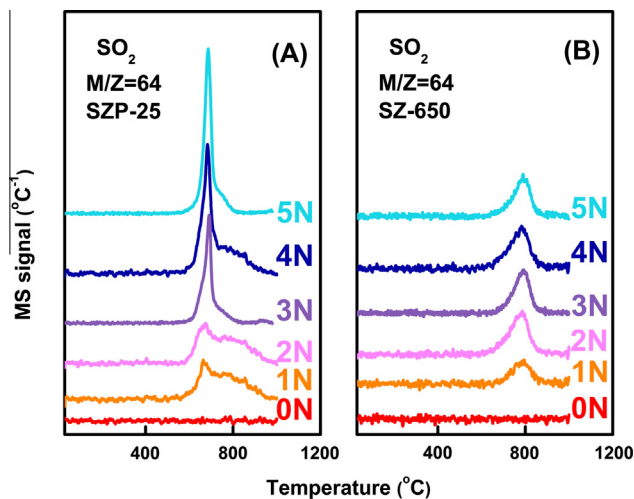
Fig. 5. SO_2 mass spectrometry (MS) signals for (A) SZP-25 and (B) SZ-650 (1–5 N) samples.
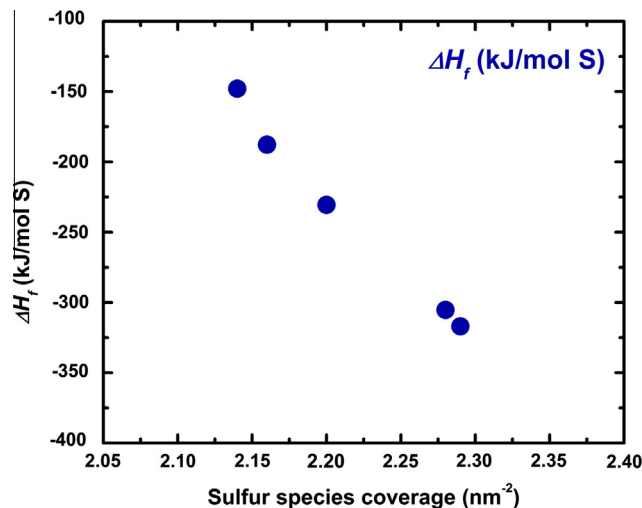

Fig. 7. Enthalpy of SZ formation from constituent oxides for SZ-650 as a function of sulfur species surface coverage.
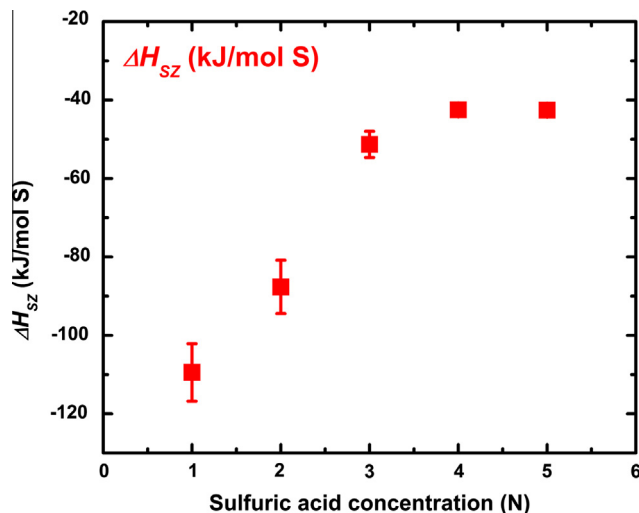

Fig. 6. Enthalpy change for sulfur species – zirconia surface interactions for SZP-25 as a function of sulfuric acid concentration.

Fig. 8. Olefin conversion rate of SZ catalyst prepared at different temperatures, from 500 to 700 °C.

there are two groups of energetically distinct sulfate species on zirconia surface as a function of sulfur loading (Fig. 2). These can be identified as the sulfate moieties directly adsorbed through chemisorption before sulfate monolayer formation, and the subsequent, presumably attached through hydrogen bonding, sulfur species beyond the monolayer. The molar ratio of monolayer sulfur to loosely attached sulfur is approximately 1:1 (Fig. 3).

4.2. Surface energetics of SZ: a function of sulfur species coverage

Despite numerous investigations, our understanding of the surface chemistry of SZ is still limited due to the intrinsic complexity
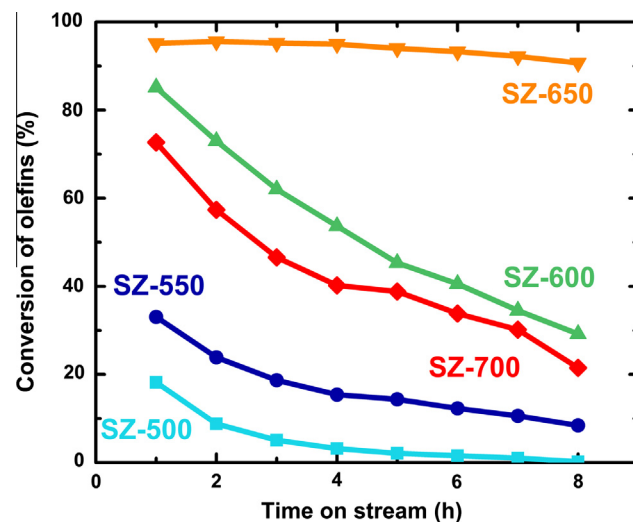
of the amorphous zirconia surface and the large variety of possible sulfur species. The thermochemical approach offers a unique angle evaluating the general behavior of a population of molecular species on complex, amorphous surfaces.

Our results are consistent with the simulation and spectroscopy. Using periodic plane wave pseudopotential calculations based on density functional theory (DFT), Haase and Sauer [15] predicted that at ultra-low coverage there would be three most stable configurations of sulfur species on different surfaces of tetragonal zirconia: a tridentate sulfate ion on the (1 0 1) surface
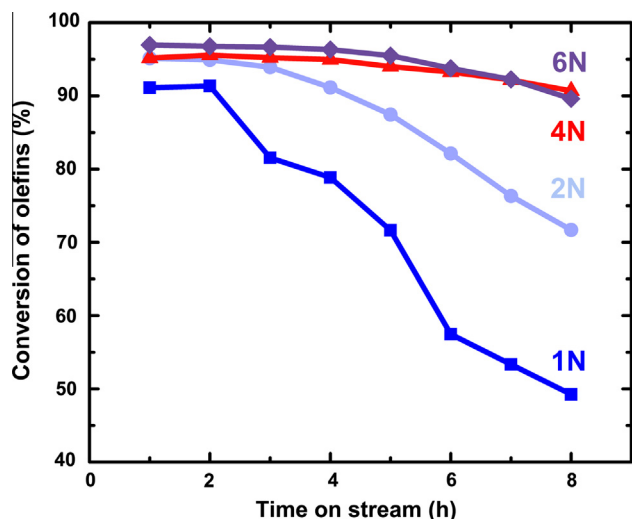
Fig. 9. Olefin conversion rate of SZ catalyst prepared under different sulfuric acid concentration, from 1 to 6 N.

(-322 kJ/mol S), a bidentate sulfate complex on the (0 0 1) surface (-408 kJ/mol S), and a SO_3 complex on the (0 0 1) surface (-467 kJ/mol S). In this case, the site-isolated monosulfates (SO_3, HSO_4^-, SO_4^{2-}) are well dispersed and directly anchored at the most strongly interacting zirconia surface sites with minimum self-interactions. Subsequently, as the surface coverage increases, sulfur species may react among themselves forming complexes and/or polysulfate species upon calcination. Employing DFT with periodic boundary conditions, Hofmann et al. [16] predicted that at relatively high coverage, as the sulfate loading reached $2H_2SO_4$ per two surface unit cells (four Zr sites), transformation from monosulfates (SO_3, HSO_4^-, SO_4^{2-}) to pyrosulfate, such as $HS_2O_7^-$ and $S_2O_7^{2-}$, might occur during calcination. Later, Hino et al. [14] carried out XPS analysis, which demonstrated that, at relatively high coverage, the active moieties on the post calcination SZ surface are polysulfate species assembled by three to four sulfur atoms. In addition to the coordination binding of S=O with Zr, these polysulfate assemblages form two S—O—Zr ionic bonds with the zirconia surface. Such a spectrum of microscopic configurations from monosulfates to polysulfates is tightly correlated to and supported by the measured heats of formation, which show increasingly exothermic formation enthalpies for SZ with higher sulfur species coverage. This may reflect favorable interactions during formation of complex more polymerized sulfur species. Interestingly, the SZ catalysts with less exothermic enthalpies of formation exhibit better conversion of olefins. This may suggest that lower thermodynamic strength of sulfur bonding both to the zirconia surface and among sulfur species may enable easier bond rearrangement and olefin accessibility during catalysis. Further spectroscopic and surface structural evidence is clearly needed to correlate the energetics with specific surface chemistry.

5. Conclusions

Using XRD, TGA-MS, immersion and high temperature oxide melt drop solution calorimetry, we performed a detailed study on the thermodynamics of two critical topics for sulfated zirconia catalysts, sulfuric acid immersion (catalyst precursor preparation) and sulfate – zirconia bonding as a function of sulfuric acid concen-

tration (C_s). The enthalpy of immersion becomes less exothermic as C_s increases, while the enthalpy of SZ formation tends to be more exothermic linearly as sulfur species coverage increases. These thermochemical insights are tightly correlated to the surface coverage and configuration of sulfur species. In a broader context, knowing such energetic insights is critical to understand catalyst synthesis and active compounds – catalyst support interactions for heterogeneous catalysts. The thermodynamic insights gained here into competitive interactions of sulfur species on zirconia surfaces may enrich our understanding of sulfated zirconia catalysts and their analogues.

Conflict of interest

The authors declare no competing financial interest.

References

[1] B.C. Gates, J. Catal. 328 (2015) 72–74.
[2] P. Serna, B.C. Gates, Acc. Chem. Res. 47 (2014) 2612–2620.
[3] M.H. Lim, C.F. Blanford, A. Stein, Chem. Mater. 10 (1998) 467–470.
[4] F.R. Chen, G. Coudurier, J.F. Joly, J.C. Vedrine, J. Catal. 143 (1993) 616–626.
[5] P. Wang, J. Zhang, G. Wang, C. Li, C. Yang, J. Catal. 338 (2016) 124–134.
[6] R.A. Keogh, D. Sparks, J.L. Hu, I. Wender, J.W. Tierney, W. Wang, B.H. Davis, Energy Fuels 8 (1994) 755–762.
[7] E. Vlasov, S. Myakin, M. Sychov, A. Aho, A.Y. Postnov, N. Mal'tseva, A. Dolgashev, S.O. Omarov, D.Y. Murzin, Catal. Lett. 145 (2015) 1651–1659.
[8] J.J. Yao, N.W. Liu, L. Shi, X. Wang, Catal. Commun. 66 (2015) 126–129.
[9] A. Koklin, V.K. Chan, V. Bogdan, Russ. J. Phys. Chem. B 8 (2014) 991–998.
[10] A. Patel, V. Brahmkhatri, N. Singh, Renewable Energy 51 (2013) 227–233.
[11] S. Ardizzone, C.L. Bianchi, Surf. Interface Anal. 30 (2000) 77–80.
[12] F. Babou, G. Coudurier, J.C. Vedrine, J. Catal. 152 (1995) 341–349.
[13] J.F. Haw, J. Zhang, K. Shimizu, T.N. Venkatraman, D.-P. Luigi, W. Song, D.H. Barich, J.B. Nicholas, J. Am. Chem. Soc. 122 (2000) 12561–12570.
[14] M. Hino, M. Kurashige, H. Matsuhashi, K. Arata, Thermochim. Acta 441 (2006) 35–41.
[15] F. Haase, J. Sauer, J. Am. Chem. Soc. 120 (1998) 13503–13512.
[16] A. Hofmann, J. Sauer, J. Phys. Chem. B 108 (2004) 14652–14662.
[17] D. Wu, S.-J. Hwang, S.I. Zones, A. Navrotsky, Proc. Natl. Acad. Sci. USA 111 (2014) 1720–1725.
[18] D. Wu, A. Navrotsky, Geochim. Cosmochim. Acta 109 (2013) 38–50.
[19] D. Wu, X. Guo, H. Sun, A. Navrotsky, J. Phys. Chem. C 119 (2015) 15428–15433.
[20] H. Sun, D. Wu, X. Guo, B. Shen, J. Liu, A. Navrotsky, J. Phys. Chem. C 118 (44) (2014) 25590–25596.
[21] D. Wu, A. Navrotsky, Proc. Natl. Acad. Sci. USA 112 (2015) 5314–5318.
[22] D. Wu, J.J. Gassensmith, D. Gouvea, S. Ushakov, J.F. Stoddart, A. Navrotsky, J. Am. Chem. Soc. 135 (2013) 6790–6793.
[23] D. Wu, T.M. McDonald, Z. Quan, S.V. Ushakov, P. Zhang, J.R. Long, A. Navrotsky, J. Mater. Chem. A 3 (2015) 4248–4254.
[24] D. Wu, X.F. Guo, H. Sun, A. Navrotsky, J. Phys. Chem. Lett. 6 (2015) 2439–2443.
[25] D. Wu, X.F. Guo, H. Sun, A. Navrotsky, J. Phys. Chem. C 120 (2016) 7562–7567.
[26] Z. Akimbekov, D. Wu, C.K. Brozek, M. Dinca, A. Navrotsky, Phys. Chem. Chem. Phys. 18 (2016) 1158–1162.
[27] A. Navrotsky, J. Am. Ceram. Soc. 97 (2014) 3349–3359.
[28] J. Majzlan, A. Navrotsky, J. Neil, Geochim. Cosmochim. Acta 66 (2002) 1839–1850.
[29] C. Drouet, A. Navrotsky, Geochim. Cosmochim. Acta 67 (2003) 2063–2076.
[30] M.W. Pitcher, S.V. Ushakov, A. Navrotsky, B.F. Woodfield, G. Li, J. Boerio-Goates, B.M. Tissue, J. Am. Ceram. Soc. 88 (2005) 160–167.
[31] N. Liu, X. Pu, L. Shi, Chem. Eng. Sci. 119 (2014) 114–123.
[32] N. Liu, X. Pu, X. Wang, L. Shi, J. Ind. Eng. Chem. 20 (2014) 2848–2857.
[33] C. Morterra, G. Cerrato, F. Pinna, M. Signoretto, J. Catal. 157 (1995) 109–123.